Carbon 142 (2019) 337–345

Contents lists available at ScienceDirect

Carbon

journal homepage: www.elsevier.com/locate/carbon

Review article

Tuning the interlayer spacing of forward osmosis membranes based on ultrathin graphene oxide to achieve desired performance

Wei-Song Hung [a, *], Yu-Hsuan Chiao [c], Arijit Sengupta [c], Ya-Wen Lin [b], S. Ranil Wickramasinghe [c], Chien-Chieh Hu [a], Hui-An Tsai [b], Kueir-Rarn Lee [b], Juin-Yih Lai [a, d]

[a] Graduate Institute of Applied Science and Technology, National Taiwan University of Science and Technology, Taipei, 10607, Taiwan
[b] R&D Centre for Membrane Technology, Chung Yuan University, Taoyuan, 32023, Taiwan
[c] Ralph E Martin College of Chemical Engineering, University of Arkansas, Fayetteville, AR, United States
[d] Department of Chemical Engineering, National Taiwan University of Science and Technology, Taipei, 10607, Taiwan

ARTICLE INFO

Article history:
Received 28 August 2018
Received in revised form
5 October 2018
Accepted 17 October 2018
Available online 18 October 2018

Keywords:
Graphene oxide
Self-assembly
FO
PRO
Crosslinking
Interlayer spacing
GO-MPD/TMC

ABSTRACT

Forward osmosis membranes based on ultrathin graphene oxide (GO) were fabricated. Suitable crosslinking agents were used to tune the interlayer spacing of GO sheets to achieve the desired membrane performance. The physicochemical properties of membranes were evaluated using different techniques. The interlayer spacing of GO-based membranes was controlled the interaction between the surface functionality of GO with the nature of crosslinking agents, such as polyvinyl alcohol, meta-phenylenediamine (MPD) and 1,3,5-benzenetricarbonyl chloride (TMC). The covalent bonds between the layer and crosslinking agents effectively suppressed the d-spacing stretching. Unlike other symmetric structures of membranes, the GO-MPD/TMC behaviour observed in the ultrathin polyamide (36 nm) asymmetric structure for the performance of pressure-retarded osmosis (PRO) mode showed the highest flux of 20.8 LMH and low reverse salt flux of 3.4 gMH. A consistent water flux for a long-term PRO operation was achieved using GO-MPD/TMC membrane (~98.7%). Therefore, the GO-MPD/TMC membrane can be used to suppress internal concentration polarisation.

© 2018 Elsevier Ltd. All rights reserved.

Contents

* Corresponding author.
E-mail address: wshung@mail.ntust.edu.tw (W.-S. Hung).

https://doi.org/10.1016/j.carbon.2018.10.058
0008-6223/© 2018 Elsevier Ltd. All rights reserved.

1. Introduction

The lack of adequate and safe water is among the most important challenge of society. However, rivers, groundwater and lakes that are the most important resources of Earth's suffer from pollution due to industrial, power plant and municipal wastes [1,2]. Meanwhile, seawater desalination and wastewater reprocess are considered as favourable clarifications to increase water supply and alleviate water scarcity worldwide by using membrane-based forward osmosis (FO) and pressure-retarded osmosis (PRO) [3,4]. Forward osmosis has also been explored for effective removal of heavy metals and also organic micro pollutants including phenol, nitrobenzene, aniline etc as an alternative to reverse osmosis [5,6]. Hence, world-wide water desalination is a challenging research; it requires joint efforts from the research community and government. The concept of the PRO is widely recognised as a potential technology for wastewater reuse and seawater desalination.

Graphene oxide (GO) is a 2D layer structured material with multiple O-containing functional groups, including hydroxyl, carboxylic acid and epoxy groups; it also has a wide range of application in the mechanical and electronic industries [7,8]. Nevertheless, GO-based membrane technology is used mainly for ionic and molecular sieving [9]. GO is an amphiphilic nanomaterial, which initially absorbs water molecules through the hydrophilic nature of the functional groups. Subsequently, the absorbed water molecules are diffused to the hydrophobic behaviour generating water channels, which may be responsible for the enhanced water permeability through GO-based membranes [10–13]. The nanochannel of ~0.3 nm of GO membrane is sufficient for the permeation of water molecules [9,11]. However, water molecules or other solvents, including constituents' ions, interact with the different functional groups present in the GO layer. Consequently, the enhanced interlayer spacing can be applied in tuning the diameter of nanochannel and the separation behaviour of GO-based membranes [14–17]. Various kinds of GO-based membranes, including thin-film composite, reverse osmosis (RO), nanofiltration (NF), microfiltration, ultrafiltration and desalination, exhibited improvement in mechanical strength, antimicrobial characteristics, selectivity, water permeability and thermal stability compared to the conventional membranes [18–21]. Hence, GO-based membranes are used to remove dyes, separate monovalent and divalent ions, efficiently capture and dehydrate solvent–water mixtures [22–30].

GO layers are usually incorporated in membranes by Langmuir–Blodgett assembly. Noncovalent bonding on inactive porous support is performed via layer by layer assembly and surface modification via covalent bonding by using different functionalities present on the GO surface, deposition on a porous support, evaporation to self-assembly and so on [22,31–36]. The laminate structure and adhesiveness are two important factors highly influenced by the nature of the porous support materials.

In the present work, we fabricated GO-based different crosslinking membranes by using the pressure-assisted self-assembly technique. The perpetration of GO, GO- polyvinyl alcohol (PVA), GO-MPD, GO-TMC and GO-MPD/TMC membranes were analysed using different techniques to characterize surface properties, such as zeta potential, X-ray photoelectron spectroscopy (XPS) and scanning electron microscopy (SEM). The GO-TMC and GO-MPD/TMC showed asymmetric behaviour, while other membranes showed symmetric properties. The effect of interlayer spacing on the overall performance of the membranes in terms of permeability and reverse salt flux (J_s) was investigated. The membrane performance was tested using a glass tube with FO/PRO cell, as shown in Fig. 1.

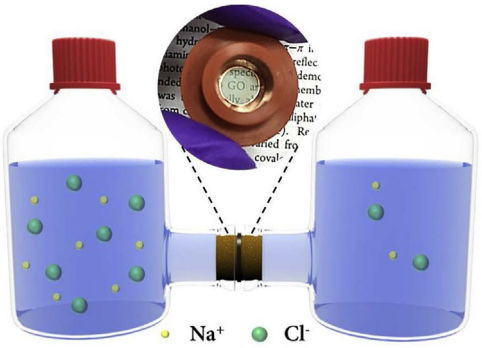

Fig. 1. Schematic experimental setup for the FO/PRO performance of the GO-based composite membranes.

2. Experimental

2.1. Materials

All the materials used in the present investigation are of analytical grade unless stated otherwise. Polyvinylidene fluoride (PVDF) membranes of with a pore size of 0.22 μm was purchased from EMD Millipore (CA, USA). 1,3,5-Benzenetricarbonyl chloride (TMC), MPD and polyvinyl alcohol were obtained from Alfa Aesar (Haverhill, MA, USA). NaCl was obtained from Nihon Shiyaku Industries Ltd. (Tokyo, Japan). Deionised (DI) water produced by Thermo Fisher 18 MΩ Barnstead Smart2Pure system (Schwerte, Germany) was used throughout the experiments.

2.2. GO membrane fabrication

GO synthesis has been described previously [32]. A mixture of 4 g graphite-concentrated H_2SO_4 and $NaNO_3$ was heated at 80 °C for 2 h, and the resulting solution was cooled down in an ice bath for 20 min. Afterwards, 16 g $KMnO_4$ was added for 2 h with constant stirring to assure homogeneous solution. The resultant solution was diluted using 400 mL of DI water, and 100 mL of 30% H_2O_2 was allowed to stand for 1 day to obtain GO sheets. Finally, the homogeneous solution was washed with HCl and DI water up to neutralise the pH. The resulting GO sheets were dried and exfoliated in DI water to prepare GO suspension by sonication.

The aqueous suspension of GO (20 mL, 25 ppm) was allowed to pass through a PVDF membrane at a pressure of 5 bar, and the GO layer was detached from PVDF support to have a symmetric GO membrane without any support layer. Thickness and size of GO nano sheet have been evaluated using the method reported in the literature using AFM (atomic force microscopic image analysis) [37]. A GO size of 4–8 μm was determined from the size distribution of several GO sheets. From the inset chart, the GO thickness (marked with blue crosses on the image) was evaluated as 1 ± 0.3 nm.

For preparation of GO-MPD and GO-PVA membranes, to an aqueous dispersion of GO (25 ppm), 25 ppm of either PVA or MPD aqueous solution was mixed and stirred for 10 min at ambient temperature in order to achieve complete homogenization. To avoid pre-crosslinking, the 20 mL mixed solution was filtrated using PVDF membrane at 5 bar and the GO membrane was air dried under room temperature. This pressure assisted self-assembled technique was followed from the literature [32]. GO-PVA, GO-MPD and GO-TMC membranes were obtained in similar fashion. For the fabrication of GO-MPD/TMC membrane, 20 mL of 25 ppm TMC in hexane solution was pressurised on GO-MPD membrane to generate the GO-MPD/TMC membrane. Freestanding GO base

membrane was stripped through a preserved hole (5 mm) with 3 M copper double-sided tape. The homogeneity and absence of any local undesired reaction resulting heterogeneous surface were checked by the scanning electron microscopic imaging (SEM).

2.3. Membrane characterisation

The dynamic water contact angle of the GO-based composite membranes (dry and wet) was measured by FACE Automatic Interfacial Tensiometer (Japan). All data were collected after 1 s time interval up to a duration of 10 s. The surface morphology and symmetric/asymmetric nature of the GO-based composite membranes were analysed by field-emission SEM (FE-SEM) by using FE-SEM Model S-4800 (Hitachi Co., Japan) with 15 kV electron beam. The XPS analysis of these GO-based composite membranes were carried out using XPS (Thermo Scientific, K-Alpha) with an Al Kα X-ray source (1486.71 eV, 5 mÁ, 15 kV) to prove crosslinking. The surface charge of these GO-based composite membranes was determined in terms of zeta potential by using dynamic light scattering (Zetasizer Nano ZS90, Malvern, United Kingdom). The flat surface cell was measured with the surface at a pH of 7 and NaCl solution for calibration to evaluate the zeta potential. To measure the interlayer spacing in GO-based composite membranes, we applied XRD technique by using wide-angle XRD (Bruker D8 ADVANCE, Germany).

2.4. Membrane performance

The feed solution was directly in contact with the membrane. The osmotic pressure difference created between the feed solution and the draw solution across the membrane is the driving force for the forward osmic separation. A 2 M NaCl solution was used as the draw solution in the FO and PRO modes for confirmation, where FO membranes was facing the dense active side of the feed solution, and the PRO mode was facing on the porous supporting layer of the feed solution. In the present studies, FO operation for the time resulting Δm of permeate corresponds to the Δv through an effective membrane surface A. The water J value can be evaluated using the equation below [38,39].

$$J = \frac{\Delta v}{A\,t} = \frac{\frac{\Delta m}{\rho}}{A\,t} \tag{1}$$

where ρ denotes the density of the feed solution at the operating temperature. The reverse J_s is a quantitative measure for the loss of selectivity of FO performance. The salt solution J across the membrane from the draw side to the feed side. The lower the value of the reverse J_s is, the better the FO performance of the membrane is. If c and v are the concentration and volume of salt in feed, then J_s can be expressed as follows [2,40].

$$J_s = \frac{c\,v}{A\,t} \tag{2}$$

The normalised water J (J_n) for the FO process by using these GO-based composite membranes can be evaluated in terms of the initial water J (J_0) and the water J at time t (J) by using the expression as follows:

$$J_N = \frac{J}{J_0} \tag{3}$$

The J_{Sp} for these GO-based composite FO membranes was determined in terms of the ratio of specific J_s to the water J, as follows:

$$J_{Sp} = \frac{J_s}{J} \tag{4}$$

3. Results and discussion

3.1. Characterization

To determine the hydrophilicity/hydrophobicity of the resulting GO-based composite membranes, we measured the dynamic water contact angles, as shown in Fig. 2 **(a)**. The water contact angles of these composite membranes followed the following trend: GO < GO-PVA < GO-MPD < GO-MPD/TMC < GO/TMC. The water contact angle was measured in the dry state of the membranes. The contact angle values clearly indicated that except for GO/TMC composite membranes, all GO-based composite membranes are highly hydrophilic in nature. Given the presence of multiple hydroxyl and carboxylic groups on the surface of GO sheets, the GO membrane is highly hydrophilic in nature. Even the presence of polar epoxy group may contribute towards the hydrophilicity of the GO membrane. However, the GO membrane shows a contact angle ranging from 42° to 47° in the GO-PVA composite membrane reported by Lecaros et al. [24] They also reported that the contact angle values increased with the increase in PVA content in the GO-PVA composite membranes and increased to more than 62° at 8 wt % PVA content in GO. Our investigation revealed that GO-PVA composite membrane possessed a water contact angle of 64°. The contact angles for GO-MPD, GO-MPD/TMC and GO/TMC were 74°, 83° and 92°, respectively. The enhancement of contact angle via the incorporation of different crosslinking agents revealed that the utilisation of −OH and −COOH groups in the GO surface of

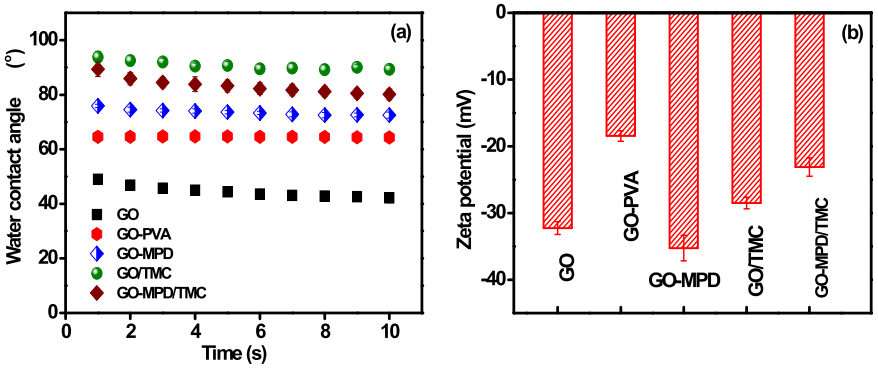

Fig. 2. Water contact angles (a) and zeta potential (b) for GO-based composite membranes with different crosslinking agents.

crosslinking agents made the membrane less hydrophilic. Park et al. [26] reported a reduction in the water contact angle by increasing the relative amount of GO in polysulfone membranes. Hung et al. [32,35] reported that the GO–cellulose acetate composite membranes with different crosslinking diamides possess contact angles ranging from 80° to 25°, thereby revealing the hydrophilic nature of these composite membranes. For GO-PVA, the alcoholic -OH groups of PVA interact with either epoxy group from GO resulting –OH and –O- moieties by opening up of epoxy ring; or reacts with –COOH groups of GO resulting ester moieties. Some unused –OH groups of PVA also add to the overall hydrophilicity of GO membrane. Therefore, by crosslinking with PVA, the water contact angle increased marginally. GO-MPD membrane, the $-NH_2$ groups from MPD were utilized either to open up epoxy ring by nucleophilic attack or amide bond formation with GO -COOH groups. Unlike PVA, no extra hydrophilic –OH groups were introduced and hence the hydrophilicity of GO-MPD is lesser compared to GO-PVA. GO/TMC and GO-TMC/MPD are asymmetric in nature. GO/TMC crosslinking occurred mainly by the reaction of –OH from GO to the acid chloride (-COCl) from TMC. Practically, for these two membranes the active surface would have more evidence of polyamide or polyester moieties.

The overall separation scheme of a membrane is highly influenced by the surface charge of the membranes [41–43]. Therefore, zeta potential was measured for GO-based composite membranes and depicted in Fig. 2 **(b)**. The zeta potential was recorder at pH 7 for all the membranes. The GO membrane possessed highly negative surface charge which can be attributed to the presence of deprotonated carboxylic groups for the zeta potential value of −32.3 mV. GO-PVA membrane showed less negative surface charge of zeta potential values of −18.5 mV than that of the GO membrane. The utilisation of –COOH groups from the GO surface formation of ester group coupling with the –OH group of PVA may be responsible for the reduction in the negative surface charge for the GO-PVA composite membrane. The GO-polyamide composite membranes also possess a negative surface charge in a pH range of 3.5–8.5. In GO-MPD, the negative surface charge of the membrane further increased compared with that of GO membrane. Although some –COOH groups from GO were utilised in the formation of amide linkage with MPD, the real reason for the enhanced negative surface charge is unknown. For other GO-based composite membranes, the reduction in the negative surface charge indicated the less availability of surface –COOH group due to its utilisation in TMC and MPD/TMC crosslinking compared with GO membranes. The GO surface function groups interacted with the –OH and $-NH_2$ groups of TMC and MPD/TMC in crosslinking, and the negative surface charges, that is −28.5 and −23.1 mV, were measured, respectively. Hence, GO/TMC and GO-MPD/TMC membranes are suitable for PRO and FO application. In GO-MPD, the negative surface charge of the membrane further increased compared with that of GO membrane. Although some –COOH groups from GO were utilized in the formation of amide linkage with MPD, the real reason for the enhanced negative surface charge is unknown.

The FTIR spectra for GO based membranes are shown in Supplementary Fig. 1. The absorption peaks at 3300, 1726, 1626, 1364, 1213, and 1029 cm^{-1} were assigned to stretching of hydroxyl (OH), carboxyl (C=O), aromatic (C=C), carboxy (C-O), epoxy (C-O), and alkoxy (C-O) groups, respectively. OH peak was found to be reduced after crosslinking. The sensitivity of FTIR is not impressive and the above spectra did not give much information on the membrane characterization. Therefore, it is essential to employ additional technique like XPS in order to proper characterization of the resulting GO based membranes.

Fig. 3 shows the XPS spectra for GO-based composite membranes. The deconvoluted XPS spectrum in the C 1s region for the GO membrane showed peaks at 288.2, 286.7, 284.6 and 285.6 eV which were assigned to –C=O, C-O-C, C-C and C-O/C-N, respectively. Similar XPS spectra in the C 1s region was also reported by Zhang et al. [25] for carboxyl-functionalised GO polyamide NF membrane, Lecaros et al. [24] for GO framework composite membrane, Hung et al. for GO-framework membranes and Zhou et al. [25] for GO-based hollow fibre membrane. For GO-PVA composite membrane, the relative intensity of 285.6 eV peak was enhances due to the presence of several hydroxyl groups from PVA moiety. Consequently, a significant reduction in the C–C peak at 284.6 eV was observed. This reduction was similar for all the composite membranes possibly due to crosslinking. A significant enhancement in the carbonyl peak intensity observed for GO/TMC and GO-MPD/TMC membranes were ascribed to the contribution from several carbonyl moieties of TMC crosslinking. The enhancement in –C=O peak was also reported by Zhang et al. [25] for their carboxylic acid-functionalised GO-based membranes. The changes in the relative intensities of diamine-based spacers/crosslinking agents in GO-based composite membranes was also previously reported by Hung et al.

As shown in Fig. 4, the SEM images of GO-based composite membranes showed the surface morphology, as well as the cross-section, of the membranes. The surface image of GO membrane showed that it possesses nodular structure which is typical for GO surface. The GO thickness was 152 nm. The cross-sectional image also clearly showed the appearance of GO sheet structure. The surface morphology changed significantly for GO composite membrane. The typical signature of crosslinking on the surface was evident. The overall thickness of the membrane increased to 222 nm; compared with GO-PVA, GO-MPD showed much similar surface morphology to that of GO membrane. This phenomenon can be easily explained by considering the fabrication mode and the size of the crosslinking agents. Given the smaller size of MPD than PVA, the applied pressure caused the MPD molecules to penetrate the pores of the GO membrane. Consequently, GO-MPD surface was similar to GO membrane. Meanwhile, successful crosslinking was evident due to the enhancement of GO-MPD membrane thickness compared with that of GO membrane. GO, GO-MPD and GO-PVA membranes were symmetric in nature, while asymmetry was introduced for GO/TMC or GO-MPD/TMC membranes because TMC is insoluble in water but soluble in organic solvent. The homogeneous distribution of GO/TMC crosslinking was evident in the surface images of GO/TMC and GO-MPD/TMC membranes. The surface morphologies of these two membranes were but distinctly different from the surface morphology of the other membranes. The active layer was found on the top of the membranes where the pressure was applied during the fabrication of GO/TMC membrane with a thickness of 193 nm. For GO-MPD/TMC membrane, the active layer with a thickness of 36 nm was observed on a regular GO membrane with a thickness of 197 nm, as well as on the typical signature of interfacial polymerisation. During capturing the cross-sectional view of GO-MPD/TMC membrane, different locations were randomly chosen in order to measure the polyamide active layer. The thickness range was evaluated in the range 30–40 nm; hence the thickness was reported as 36 ± 5 nm. The overall SEM analysis also revealed an enhancement in the GO membrane thickness during crosslinking, thereby enhancing the d-spacing between different GO sheets due to crosslinking. Although similar enhancement in the d-spacing was also observed by the incorporation of diamine-based crosslinking agents into GO membranes, systematic X-ray diffraction (XRD) analysis is essential.

It is also required to mention that due to the presence of 36 nm thick active layer in GO-MPD/TMC membrane, the surface characterization of this asymmetric membrane mostly evidenced the signature of polyamide surface formed by MPD and TMC. The water

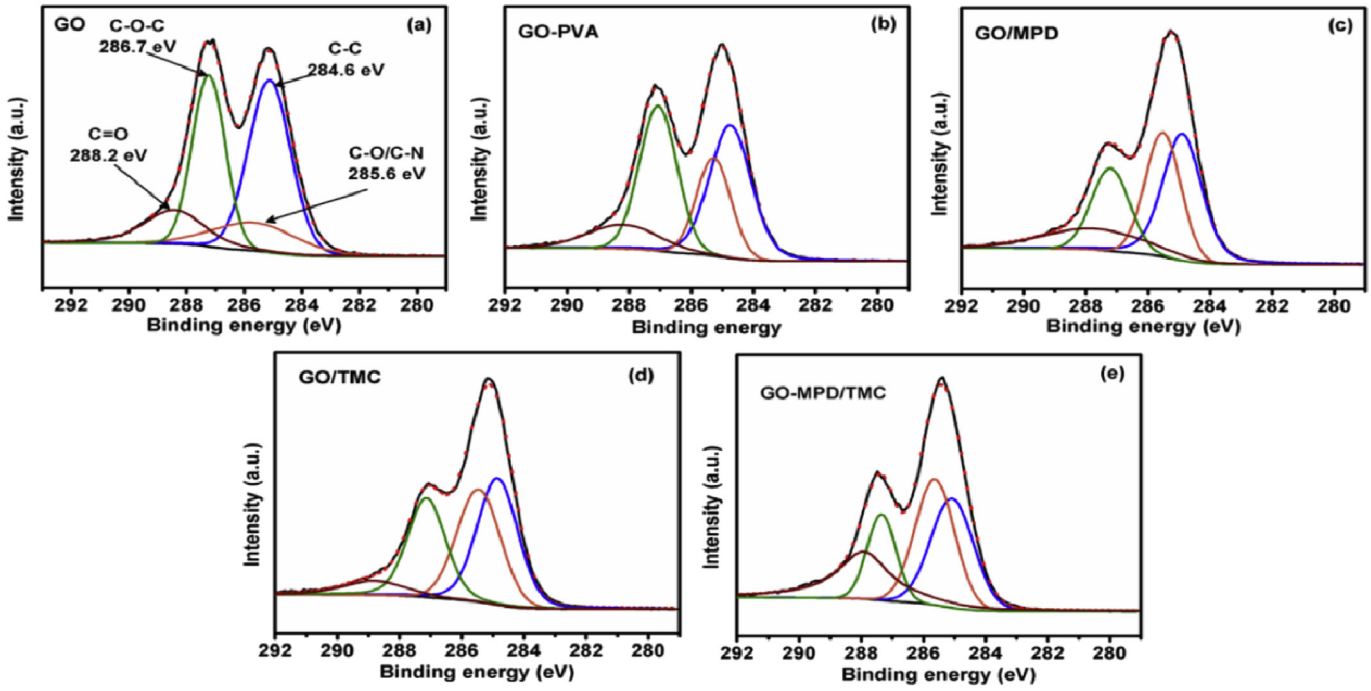

Fig. 3. XPS spectra for GO-based composite membranes, including (a) GO, (b) GO-PVA, (c) GO-MPD, (d) GO/TMC and (e) GO-MPD/TMC membranes.

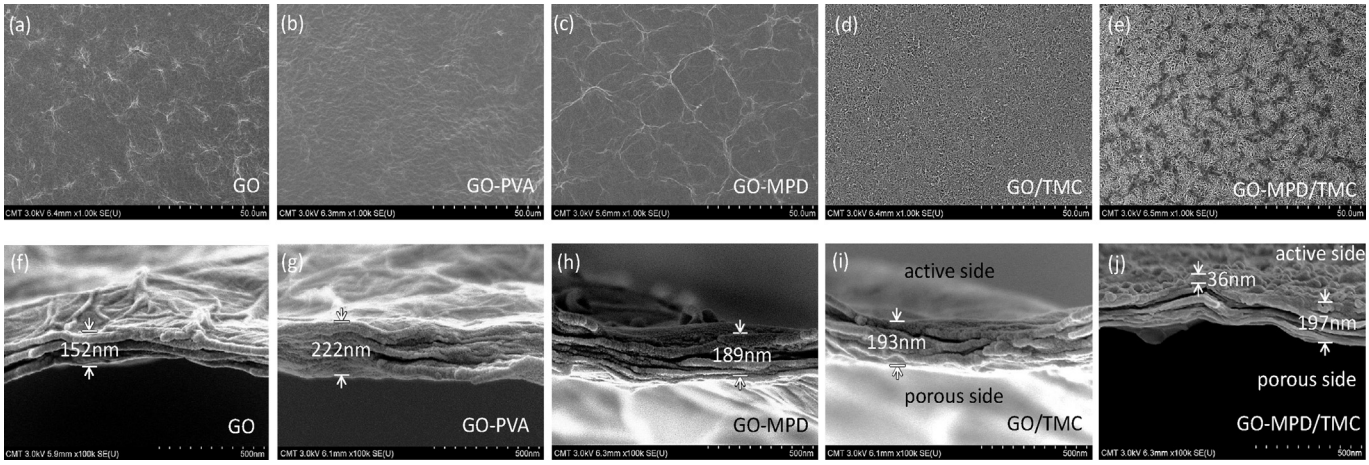

Fig. 4. SEM images for GO-based composite membranes; (a–e) surface; (f–j) cross-sectional view: (a, f) GO; (b, g) GO-PVA; (c, h) GO-MPD; (d, i) GO/TMC; and (e, j) GO-MPD/TMC.

contact angle of 83° and zeta potential of − 24 mV are mostly due to the polyamide active layer. The relative enhancement in the 288.2 eV and 285.6 eV peaks in deconvoluted XPS spectra for this asymmetric membrane also suggested the enhancement of carbonyl (C=O) and (C-N) bonds on the active side of the membrane surface. Both of these bonds are expected from the amide functionality of polyamide layer formed by coupling of TMC and MPD.

Fig. 5 shows the XRD pattern for GO-based membranes in dry, as well as wet, condition. An aqueous solution of 2 M NaCl was used for wet condition to mimic effect of draw solution on the d-spacing of GO layers. For asymmetric membranes the active layers were subjected to the investigation. In the dry state, the GO membrane possessed the d-spacing of 0.85 nm which is similar to that reported in our previous investigations [24,32]. The slight change either can attribute to the different mode of preparation of the GO membrane or may be within the error limit, as shown in Fig. 5 **(a, c)**. The wet state of the d-spacing GO membrane increased due to the penetration of water molecules and salt ions between the layers. Similar enhancement in the d-spacing was also reported in the literature. The extent of enhancement in the d-spacing was dependent on the interaction between the solvent molecules containing ions and the GO sheets, as shown in Fig. 5 **(b, c)**. In the present study, the enhancement in the d-spacing was due to the electrostatic interaction between H_2O molecules, Na^+ and Cl^- ions with −COOH and epoxy groups from GO sheets. The crosslinking agents showed enhanced d-spacing behaviour utilised in suitable tuning of the interlayer spacing in GO-based membranes, and GO composites membrane achieved either flux (J) improvement or rejection.

The GO composite membrane prepared in dry condition showed the following d-spacing trend: GO < GO-MPD/TMC < GO-

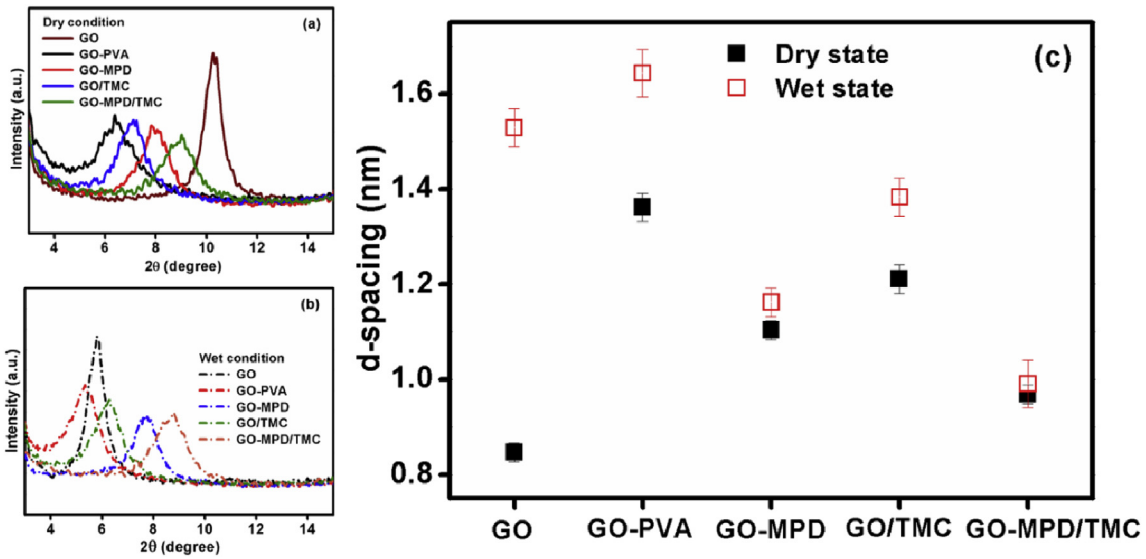

Fig. 5. **(a–c)** XRD analysis for GO-based composite membrane in dry and wet conditions in understanding the d-spacing between GO sheets.

MPD < GO/TMC < GO-PVA, respectively. The largest d-spacing for GO-PVA can be attributed to the bridging of polymer molecules between two GO sheets. The opening of the strained epoxy ring of GO surface interacted with the nucleophilic attack of −OH groups from the PVA polymer. The wet condition for GO-PVA membranes enhanced the interlayer spacing possibly due to the swelling of bridged PVA polymer molecules apart from the conventional solvent−GO interaction. In GO-MPD membrane, an amide linkage $-NH_2$ group of MPD was observed between the −COOH group of the GO surface, and the epoxy ring opening into the nucleophilic attack of $-NH_2$ group of MPD may be responsible for the enhanced interlayer spacing. GO sheet interaction was modified, thereby resulting in decreased interaction with the solvent molecules in wet state. Hence, only marginal enhancement in the d-spacing of GO-MPD membrane was observed in the wet condition compared with dry condition. GO/TMC and GO-MPD/TMC membranes exhibited asymmetric membrane synthesis strategy, as shown in the SEM image. The acid chloride (−COCl) groups of TMC were not expected the form any strong bond between the two consecutive layers of GO. Therefore, the slight enhancement in TMC was associated with the GO membrane and the TMC molecules between the two layers of GO membrane due to high pressure fabrication. The membrane in the wet state showed enhancement in the interlayer spacing of GO/TMC membrane. GO-MPD/TMC and GO-MPD membranes were also fabricated in an aqueous medium, followed by pressurising of TMC in an organic medium. The both phases were utilised to result in the asymmetric behaviour of GO-MPD/TMC membrane. The interlayer spacing between both conditions (dry, wet) also revealed the compression of GO-MPD/TMC membrane. The simplified chemical structures of these GO composite membranes are depicted in Fig. 6, as follows:

3.2. Membrane performance

An overall performance of GO composite membrane was used carried out the operation for 6 h by using the FO, RO and long-term stability, as shown in Fig. 7. The FO modes, as well as the PRO modes, were evaluated in terms of the water J, reverse J_s and specific J (J_{Sp}). As shown in Fig. 7 **(a, b)**, the water J in both modes followed the trend as follows: GO < GO-PVA < GO/TMC < GO-MPD < GO-MPD/TMC. The reverse J_s values showed the trend as follows: GO > GO-PVA > GO/TMC > GO-MPD > GO-MPD/TMC. Interlayer spacing highly influenced the penetration of water molecules across the membrane. The observed water flux is the resultant of two counter motion: motion of water molecules from feed to permeate side and motion of the ions of the salt from permeate to feed side. For dense membrane, the contribution of the 2nd factor is insignificant, while with increase in porosity of the membrane, the 2nd factor contributes. The observed water flux is the resultant of two counter motion: motion of water molecules from feed to permeate side and motion of the ions of the salt from permeate to feed side. For dense membrane, the contribution of the 2nd factor is insignificant, while with increase in porosity of the membrane, the 2nd factor contributes. The enhancement in d-spacing increased the motion of water molecules, but the flow of salt from the draw side to the feed side also increased. Therefore, the interlayer spacing favored both motions which are directed oppositely, that is the motion of water molecules from the feed side to the draw solution side and the motion of salt ions from the draw solution side to the feed side. Consequently, the observed water J was a result of these two counter motions. As shown in Fig. 7 **(c)**, J_{Sp} followed the trend: GO > GO-PVA > GO/TMC > GO-MPD > GO-MPD/TMC. The water J values of GO, GO-MPD and GO-PVA membranes were similar in both FO and PRO modes. In the FO mode, the dense active layer faced the feed solution, and the PRO mode is the porous supporting layer facing the feed solution. Similar J values were observed for GO, GO-PVA and GO-MPD membranes in both modes in terms of symmetric behaviour and GO/TMC and GO-MPD/TMC membranes in terms of asymmetric nature which were also concluded from the SEM image analysis. By contrast, the GO/TMC and GO-MPD/TMC membrane performances of the water J values for PRO mode were higher than those for FO mode which was in accordance with our hypothesis.

These two oppositely directed motions can also be evidenced by determining the water J as a function for up to 6 h. A drastic decrease in water J for GO membrane was attributed predominantly to reverse J_s in the wet state which created obstacles in the motion of water molecules from the feed to the permeate stream. A similar reduction in water J with time was observed for GO/TMC membrane. Long-term experiments showed a particular trend. The membrane with significantly different d-spacing between dry and wet states was high showed high reduction in water J during a long-

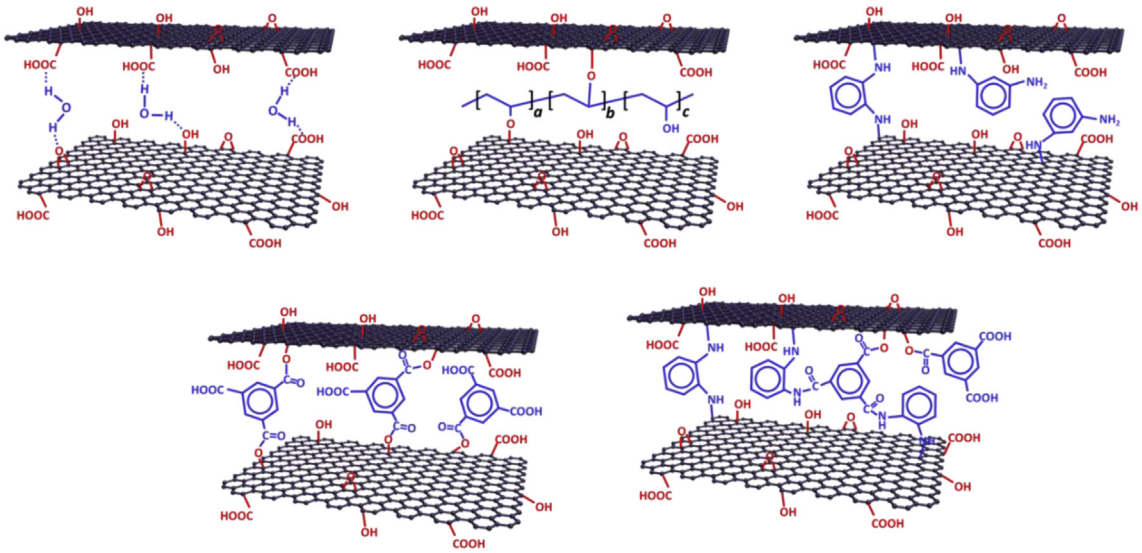

Fig. 6. Simplified chemical structure of GO-based composite membrane.

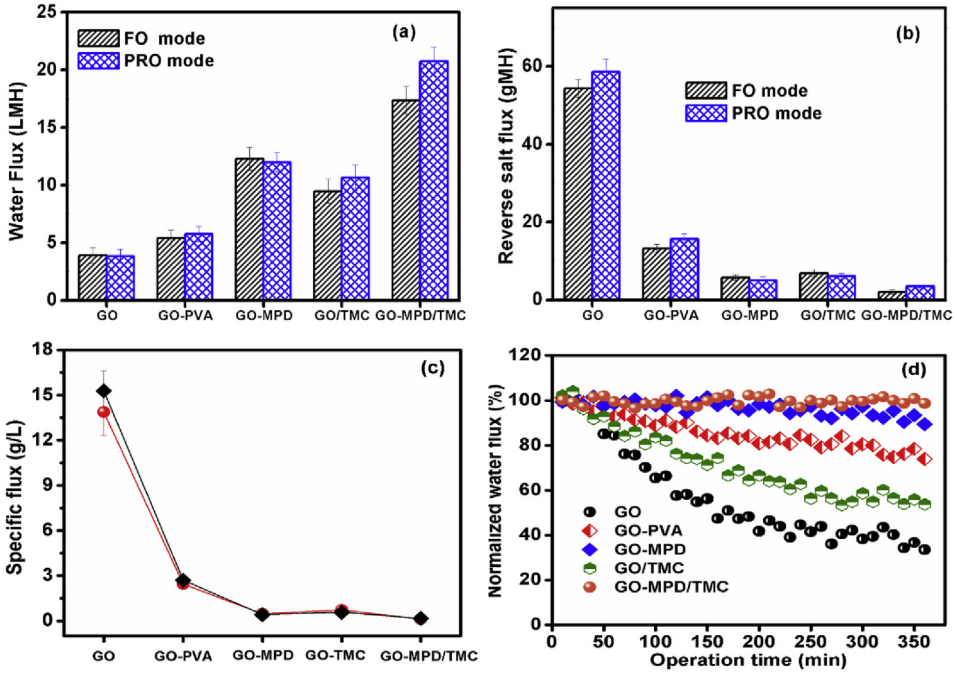

Fig. 7. Performance of GO-based membranes in terms of (a) water flux, (b) reverse salt flux, (c) specific flux and (d) normalised flux as a function of time (up to 6 h).

term FO operation. Therefore, the asymmetric membrane GO-MPD/TMC and symmetric membrane GO-MPD showed stable J for almost all throughout the operation for 6 h.

The severe internal concentration polarization was reported to be responsible for lowering the permeate flux in FO mode compared to PRO mode. Hence the flux in PRO mode was found to be 1.6–2 times more compared to that of FO mode [44–48]. In view of this, the observed lower flux value in FO mode was referred to internal concentration polarization. For the asymmetric membrane, two orientations of the membrane are studied: one with the active layer facing the feed solution (FO mode) and the other with the active layer facing the draw solution (PRO mode). When the feed solution is against the active layer and the draw solution is against the backing layer, as in the case of FO desalination, the ICP phenomenon now occurs on the permeate side. We refer to this as dilutive ICP since the draw solution is diluted by the permeate water within the porous support of the membrane [49]. In view of this, the observed lower flux value in FO mode for present investigation was referred to internal concentration polarization. Moreover, in present investigation the flux value in PRO mode is 1.15 times than that in FO mode. This clearly indicates that there is suppression of ICP, i.e. from 1.60 to 2.00 times to 1.15 times.

4. Conclusion

GO interacting with different crosslinking agents (i.e. PVA, MPD and TMC) were used to fabricate the symmetric membrane, and composite membranes were used to carry out FO and PRO studies

for up to 6 h. The composite membranes were confirmed using various techniques for the physicochemical properties, and these results confirmed to the successfully fabricated membrane. However, this result was attributable to the utilisation of hydroxyl and carboxylic acid groups on the surface of GO interacting with the different crosslinking agents. GO-PVA, GO-MPD, GO/TMC and GO-MPD/TMC membranes enhanced the water contact angle, consequently reducing the hydrophilicity of the membrane. XRD analysis was also carried out to study the d-spacing between two consecutive layers of GO membranes in dry, as well as in wet, state. Large interlayer spacing did not only facilitate the movement of water from the feed side to the permeate side but also the salt from the draw solution side to the feed side. These mutually opposite motions determined the overall water J of the composite membranes. Long-term membrane operation also revealed that GO-MPD/TMC and GO-MPD membranes exhibited stable water J in FO mode for 6 h. Given that GO, GO-PVA and GO-MPD are symmetric membranes, both FO and PRO modes showed similar water J values, while GO/TMC and GO-MPD/TMC membranes on the PRO mode showed higher J PRO values than FO mode values. GO-MPD/TMC composite membrane achieved the higher J PRO mode values than the FO values in the water desalination. It can also suppress internal concentration polarisation remarkably.

Acknowledgements

The authors would like to thank the Ministry of Science and Technology of Taiwan (grant nos. MOST 105-2221-E-011-168-MY3, 107-2218-E-011-011 and 107-2622-E-011-022-CC3) for providing financially support to this research, and the National Science Foundation Divison of Industrial Innovation & Partnership Grant No. 1848682 (USA).

Appendix A. Supplementary data

Supplementary data to this article can be found online at https://doi.org/10.1016/j.carbon.2018.10.058.

References

[1] S. Zhao, L. Zou, C.Y. Tang, D. Mulcahy, Recent developments in forward osmosis: opportunities and challenges, J. Membr. Sci. 396 (2012) 1–21, https://doi.org/10.1016/j.memsci.2011.12.023.
[2] T.Y. Cath, A.E. Childress, M. Elimelech, Forward osmosis: principles, applications, and recent developments, J. Membr. Sci. 281 (2006) 70–87, https://doi.org/10.1016/j.memsci.2006.05.048.
[3] S. Lee, C. Boo, M. Elimelech, S. Hong, Comparison of fouling behavior in forward osmosis (FO) and reverse osmosis (RO), J. Membr. Sci. 365 (2010) 34–39, https://doi.org/10.1016/j.memsci.2010.08.036.
[4] I.L. Alsvik, M.B. Hägg, Pressure retarded osmosis and forward osmosis membranes: materials and methods, Polymers (Basel) 5 (2013) 303–327, https://doi.org/10.3390/polym5010303.
[5] Y. Cui, Q. Ge, X.Y. Liu, T.S. Chung, Novel forward osmosis process to effectively remove heavy metal ions, J. Membr. Sci. 467 (2014) 188–194, https://doi.org/10.1016/j.memsci.2014.05.034.
[6] Y. Cui, X.Y. Liu, T.S. Chung, M. Weber, C. Staudt, C. Maletzko, Removal of organic micro-pollutants (phenol, aniline and nitrobenzene) via forward osmosis (FO) process: evaluation of FO as an alternative method to reverse osmosis (RO), Water Res. 91 (2016) 104–114, https://doi.org/10.1016/j.watres.2016.01.001.
[7] Y. Zhu, S. Murali, W. Cai, X. Li, J.W. Suk, J.R. Potts, R.S. Ruoff, Graphene and graphene oxide: synthesis, properties, and applications, Adv. Mater. 22 (2010) 3906–3924, https://doi.org/10.1002/adma.201001068.
[8] D. Pacilé, J.C. Meyer, A. Fraile Rodríguez, M. Papagno, C. Gómez-Navarro, R.S. Sundaram, M. Burghard, K. Kern, C. Carbone, U. Kaiser, Electronic properties and atomic structure of graphene oxide membranes, Carbon N. Y. 49 (2011) 966–972, https://doi.org/10.1016/j.carbon.2010.09.063.
[9] B. Mi, Graphene oxide membranes for ionic and molecular sieving, Science 343 (2014) 740–742, https://doi.org/10.1126/science.1250247 (80-.).
[10] T.H. Tight, Unimpeded permeation of water, Science 335 (2012) 442–444, https://doi.org/10.1126/science.1211694 (80-.).
[11] R.K. Joshi, P. Carbone, F.C. Wang, V.G. Kravets, A.K. Geim, R.R. Nair, Precise and ultrafast molecular oxide membranes, Science 343 (2014) 752–755, https://doi.org/10.1126/science.1245711 (80-.).
[12] D.W. Boukhvalov, M.I. Katsnelson, Y.W. Son, Origin of anomalous water permeation through graphene oxide membrane, Nano Lett. 13 (2013) 3930–3935, https://doi.org/10.1021/nl4020292.
[13] M. Hu, B. Mi, Enabling graphene oxide nanosheets as water separation membranes, Environ. Sci. Technol. 47 (2013) 3715–3723, https://doi.org/10.1021/es400571g.
[14] J. Zhang, Z. Xu, M. Shan, B. Zhou, Y. Li, B. Li, J. Niu, X. Qian, Synergetic effects of oxidized carbon nanotubes and graphene oxide on fouling control and anti-fouling mechanism of polyvinylidene fluoride ultrafiltration membranes, J. Membr. Sci. 448 (2013) 81–92, https://doi.org/10.1016/j.memsci.2013.07.064.
[15] Y. Heo, H. Im, J. Kim, The effect of sulfonated graphene oxide on Sulfonated Poly (Ether Ether Ketone) membrane for direct methanol fuel cells, J. Membr. Sci. 425–426 (2013) 11–22, https://doi.org/10.1016/j.memsci.2012.09.019.
[16] W. Choi, J. Choi, J. Bang, J.H. Lee, Layer-by-layer assembly of graphene oxide nanosheets on polyamide membranes for durable reverse-osmosis applications, ACS Appl. Mater. Interfaces 5 (2013) 12510–12519, https://doi.org/10.1021/am403790s.
[17] C. Xu, A. Cui, Y. Xu, X. Fu, Graphene oxide-TiO2composite filtration membranes and their potential application for water purification, Carbon N. Y. 62 (2013) 465–471, https://doi.org/10.1016/j.carbon.2013.06.035.
[18] H.R. Chae, J. Lee, C.H. Lee, I.C. Kim, P.K. Park, Graphene oxide-embedded thin-film composite reverse osmosis membrane with high flux, anti-biofouling, and chlorine resistance, J. Membr. Sci. 483 (2015) 128–135, https://doi.org/10.1016/j.memsci.2015.02.045.
[19] J.J. Song, Y. Huang, S.W. Nam, M. Yu, J. Heo, N. Her, J.R.V. Flora, Y. Yoon, Ultrathin graphene oxide membranes for the removal of humic acid, Separ. Purif. Technol. 144 (2015) 162–167, https://doi.org/10.1016/j.seppur.2015.02.032.
[20] Z.B. Zhang, J.J. Wu, Y. Su, J. Zhou, Y. Gao, H.Y. Yu, J.S. Gu, Layer-by-layer assembly of graphene oxide on polypropylene macroporous membranes via click chemistry to improve antibacterial and antifouling performance, Appl. Surf. Sci. 332 (2015) 300–307, https://doi.org/10.1016/j.apsusc.2015.01.193.
[21] Q. Nan, P. Li, B. Cao, Fabrication of positively charged nanofiltration membrane via the layer-by-layer assembly of graphene oxide and polyethylenimine for desalination, Appl. Surf. Sci. 387 (2016) 521–528, https://doi.org/10.1016/j.apsusc.2016.06.150.
[22] H.M. Hegab, L. Zou, Graphene oxide-assisted membranes: fabrication and potential applications in desalination and water purification, J. Membr. Sci. 484 (2015) 95–106, https://doi.org/10.1016/j.memsci.2015.03.011.
[23] F. Zhou, H.N. Tien, W.L. Xu, J.T. Chen, Q. Liu, E. Hicks, M. Fathizadeh, S. Li, M. Yu, Ultrathin graphene oxide-based hollow fiber membranes with brush-like CO2-philic agent for highly efficient CO2capture, Nat. Commun. 8 (2017), https://doi.org/10.1038/s41467-017-02318-1.
[24] R.L.G. Lecaros, G.E.J. Mendoza, W.S. Hung, Q.F. An, A.R. Caparanga, H.A. Tsai, C.C. Hu, K.R. Lee, J.Y. Lai, Tunable interlayer spacing of composite graphene oxide-framework membrane for acetic acid dehydration, Carbon N. Y. 123 (2017) 660–667, https://doi.org/10.1016/j.carbon.2017.08.019.
[25] H. Zhang, Bin Li, J. Pan, Y. Qi, J. Shen, C. Gao, B. Van der Bruggen, Carboxyl-functionalized graphene oxide polyamide nanofiltration membrane for desalination of dye solutions containing monovalent salt, J. Membr. Sci. 539 (2017) 128–137, https://doi.org/10.1016/j.memsci.2017.05.075.
[26] M.J. Park, S. Phuntsho, T. He, G.M. Nisola, L.D. Tijing, X.M. Li, G. Chen, W.J. Chung, H.K. Shon, Graphene oxide incorporated polysulfone substrate for the fabrication of flat-sheet thin-film composite forward osmosis membranes, J. Membr. Sci. 493 (2015) 496–507, https://doi.org/10.1016/j.memsci.2015.06.053.
[27] L. Shao, X. Cheng, Z. Wang, J. Ma, Z. Guo, Tuning the performance of polypyrrole-based solvent-resistant composite nanofiltration membranes by optimizing polymerization conditions and incorporating graphene oxide, J. Membr. Sci. 452 (2014) 82–89, https://doi.org/10.1016/j.memsci.2013.10.021.
[28] S. Zinadini, A.A. Zinatizadeh, M. Rahimi, V. Vatanpour, H. Zangeneh, Preparation of a novel antifouling mixed matrix PES membrane by embedding graphene oxide nanoplates, J. Membr. Sci. 453 (2014) 292–301, https://doi.org/10.1016/j.memsci.2013.10.070.
[29] B. Li, Y. Cui, S. Japip, Z. Thong, T.S. Chung, Graphene oxide (GO) laminar membranes for concentrating pharmaceuticals and food additives in organic solvents, Carbon N. Y. 130 (2018) 503–514, https://doi.org/10.1016/j.carbon.2018.01.040.
[30] D. Hua, T.S. Chung, Polyelectrolyte functionalized lamellar graphene oxide membranes on polypropylene support for organic solvent nanofiltration, Carbon N. Y. 122 (2017) 604–613, https://doi.org/10.1016/j.carbon.2017.07.011.
[31] L. Somers, High Yield Preparation of Macroscopic Graphene Oxide Membranes High Yield Preparation of Macroscopic Graphene Oxide Membranes, 2015, pp. 9–11, https://doi.org/10.1021/ja807934n.
[32] W.S. Hung, Q.F. An, M. De Guzman, H.Y. Lin, S.H. Huang, W.R. Liu, C.C. Hu, K.R. Lee, J.Y. Lai, Pressure-assisted self-assembly technique for fabricating composite membranes consisting of highly ordered selective laminate layers of amphiphilic graphene oxide, Carbon N. Y. 68 (2014) 670–677, https://doi.org/10.1016/j.carbon.2013.11.048.
[33] J.-T. Chen, Y.-J. Fu, Q.-F. An, S.-C. Lo, S.-H. Huang, W.-S. Hung, C.-C. Hu, K.-

R. Lee, J.-Y. Lai, Tuning nanostructure of graphene oxide/polyelectrolyte LbL assemblies by controlling pH of GO suspension to fabricate transparent and super gas barrier films, Nanoscale 5 (2013) 9081, https://doi.org/10.1039/c3nr02845c.

[34] Y. Dong, J. Shao, C. Chen, H. Li, R. Wang, Y. Chi, X. Lin, G. Chen, Blue luminescent graphene quantum dots and graphene oxide prepared by tuning the carbonization degree of citric acid, Carbon N. Y. 50 (2012) 4738–4743, https://doi.org/10.1016/j.carbon.2012.06.002.

[35] W.-S. Hung, C.-H. Tsou, M. De Guzman, Q.-F. An, Y.-L. Liu, Y.-M. Zhang, C.-C. Hu, K.-R. Lee, J.-Y. Lai, Cross-linking with diamine monomers to prepare composite graphene oxide-framework membranes with varying d-spacing, Chem. Mater. (2014), https://doi.org/10.1021/cm5007873.

[36] T. Wang, J. Lu, L. Mao, Z. Wang, Electric field assisted layer-by-layer assembly of graphene oxide containing nanofiltration membrane, J. Membr. Sci. 515 (2016) 125–133, https://doi.org/10.1016/j.memsci.2016.05.053.

[37] C.H. Tsou, Q.F. An, S.C. Lo, M. De Guzman, W.S. Hung, C.C. Hu, K.R. Lee, J.Y. Lai, Effect of microstructure of graphene oxide fabricated through different self-assembly techniques on 1-butanol dehydration, J. Membr. Sci. 477 (2015) 93–100, https://doi.org/10.1016/j.memsci.2014.12.039.

[38] W. Phillip, J.S. Yong, M. Elimelech, Reverse draw solute flux in forward osmosis modules: modeling and experiments, Environ. Sci. Technol. 44 (2010) 5170–5176.

[39] A. Soroush, W. Ma, Y. Silvino, M.S. Rahaman, Surface modification of thin film composite forward osmosis membrane by silver-decorated graphene-oxide nanosheets, Environ. Sci. Nano. 2 (2015) 395–405, https://doi.org/10.1039/c5en00086f.

[40] C.Y. Tang, Q. She, W.C.L. Lay, R. Wang, A.G. Fane, Coupled effects of internal concentration polarization and fouling on flux behavior of forward osmosis membranes during humic acid filtration, J. Membr. Sci. 354 (2010) 123–133, https://doi.org/10.1016/j.memsci.2010.02.059.

[41] M. Jebur, A. Sengupta, Y.H. Chiao, M. Kamaz, X. Qian, R. Wickramasinghe, Pi electron cloud mediated separation of aromatics using supported ionic liquid (SIL) membrane having antibacterial activity, J. Membr. Sci. 556 (2018) 1–11, https://doi.org/10.1016/j.memsci.2018.03.064.

[42] A.M. Avram, P. Ahmadiannamini, A. Vu, X. Qian, A. Sengupta, S.R. Wickramasinghe, Polyelectrolyte multilayer modified nanofiltration membranes for the recovery of ionic liquid from dilute aqueous solutions, J. Appl. Polym. Sci. 134 (2017), https://doi.org/10.1002/app.45349.

[43] M. Kamaz, P. Rocha, A. Sengupta, X. Qian, R.S. Wickramasinghe, Efficient removal of chemically toxic dyes using microorganism from activated sludge: understanding sorption mechanism, kinetics, and associated thermodynamics, Separ. Sci. Technol. 00 (2018) 1–17, https://doi.org/10.1080/01496395.2018.1440305.

[44] L. Jin, Z. Wang, S. Zheng, B. Mi, Polyamide-crosslinked graphene oxide membrane for forward osmosis, J. Membr. Sci. 545 (2018) 11–18, https://doi.org/10.1016/j.memsci.2017.09.023.

[45] H. Guo, Z. Yao, J. Wang, Z. Yang, X. Ma, C.Y. Tang, Polydopamine coating on a thin film composite forward osmosis membrane for enhanced mass transport and antifouling performance, J. Membr. Sci. 551 (2018) 234–242, https://doi.org/10.1016/j.memsci.2018.01.043.

[46] T.Y. Cath, M. Elimelech, J.R. McCutcheon, R.L. McGinnis, A. Achilli, D. Anastasio, A.R. Brady, A.E. Childress, I.V. Farr, N.T. Hancock, J. Lampi, L.D. Nghiem, M. Xie, N.Y. Yip, Standard methodology for evaluating membrane performance in osmotically driven membrane processes, Desalination 312 (2013) 31–38, https://doi.org/10.1016/j.desal.2012.07.005.

[47] L. Shen, S. Xiong, Y. Wang, Graphene oxide incorporated thin-film composite membranes for forward osmosis applications, Chem. Eng. Sci. 143 (2016) 194–205, https://doi.org/10.1016/j.ces.2015.12.029.

[48] L. Shen, J. Zuo, Y. Wang, Tris(2-aminoethyl)amine in-situ modified thin-film composite membranes for forward osmosis applications, J. Membr. Sci. 537 (2017) 186–201, https://doi.org/10.1016/j.memsci.2017.05.035.

[49] J.R. McCutcheon, M. Elimelech, Influence of concentrative and dilutive internal concentration polarization on flux behavior in forward osmosis, J. Membr. Sci. 284 (2006) 237–247, https://doi.org/10.1016/j.memsci.2006.07.049.